Interatomic Auger transitions in ionic compounds

P. H. Citrin, J. E. Rowe, and S. B. Christman
Bell Laboratories, Murray Hill, New Jersey 07974
(Received 10 March 1976)

Interatomic Auger transitions associated with valence electrons from nearest-neighbor atoms to the initial hole-state site have been measured in the ionic compounds NaF, MgF_2, and Al_2O_3. Both low- (< 100 eV) and high-(> 1000 eV) energy interatomic transitions were observed, corresponding to decay of shallow and deep core hole states, respectively. Of the former group, transitions were identified in which the final states are characterized either by a single vacancy on a site adjacent to the initial hole-state site (interatomic Coster-Kronig decay), by double vacancies localized on an adjacent site, or by double vacancies delocalized on different adjacent sites. A simple model for calculating the energies of these transitions is presented in which corrections assuming complete ionicity and dielectric response are added to empirically determined one-electron binding energies. The corrections take into account the additional electronic polarization and hole-hole interaction energies absent in single-vacancy final states. Electron binding energies measured by x-ray photoemission were self-consistently referenced to the measured kinetic Auger energies from the ionic compounds. These latter energies were then compared with those calculated using the simple model. For both high- and low-energy interatomic transitions the overall agreement, typically in the range of 1–2 eV, was within the uncertainties of the Auger measurements and comparable to that found in the studies of intra-atomic core-level transitions.

I. INTRODUCTION

Chemical effects in Auger electron spectroscopy (AES) have until only recently been a subject of qualitative understanding.[1] Such effects in AES are of two types, those in which core holes decay via lesser bound core electrons or those involving valence-electron decay directly. The former class of transitions have been most studied because of favorable intensity and signal-to-background ratios found at higher Auger electron energies. Common features found in such spectra, e.g., the *LMM* transitions in Zn and ZnO,[2] are similar multiplet structures but with sizeable chemical shifts between metal and oxide. To within 1–2 eV, the core-level phenomenology is presently understood.

The second class of Auger transitions involving the valence electrons have received only minor attention and it is their origin and interpretation with which this present work is concerned.[3] We refer to these transitions as interatomic to distinguish them from the intra-atomic core-level transitions cited above; the term crossover transitions would also be appropriate. The major distinction implied between intra- and interatomic transitions is that the latter involve valence electrons derived from atoms or ions not containing the initial core vacancy.

At first glance it is perhaps easy to understand why interatomic transitions have previously been so little studied. The low-energy regime of the Auger spectrum in which these transitions occur, < 100 eV, usually contains many transitions on top of a rapidly varying secondary electron background, thereby making reliable data acquisition somewhat difficult. The signal superposed on the background is fairly complicated because the shapes, energies, and number of peaks from one compound to another vary with the changing valence-electron distributions. These facts impose the need for understanding hole-hole interaction and one-electron binding energies somewhat more thoroughly than is normally required for interpretation of conventional intra-atomic core Auger transitions.

Weighing against these apparent difficulties are a number of reasons why investigating chemically dependent interatomic transitions is both timely and worthwhile. Recent technological improvements in Auger electron spectroscopy and the complementary technique of x-ray photoemission spectroscopy (XPS) enable the acquisition of reliable Auger spectra and electron binding energies almost routinely, thus relieving a number of previously bothersome experimental constraints. From a fundamental point of view, Auger decay is the principal annihilation mechanism for holes with energy < 2 keV,[4] so that chemical variations in interatomic Auger transitions ultimately determine chemical dependences of certain hole-state lifetimes. These, in turn, help explain basic spectral features such as linewidths and intensities of satellites in AES, as well as in XPS and x-ray emission spectroscopy.[3] Understanding the effects of chemical environment also aids in interpreting chemical shifts in all three spectros-

copies and sheds light on questions of hole-hole interaction and relaxation energies alluded to previously. Finally, the surface sensitivity of AES makes it almost imperative to understand the details of how subtle environmental changes may yield information regarding surface analyses.

The present work considers both low- and high-energy interatomic Auger transitions in ionic crystals using Auger and x-ray photoemission techniques applied to three ionic compounds, NaF, MgF_2, and Al_2O_3. Using empirical one-electron binding energies and assuming complete ionicity, the Auger energies for energetically allowed interatomic transitions are calculated and compared with experiment. The simple ionic model is shown to predict Auger energies typically to within the ±1.5-eV range of experimental uncertainties found in our measurements, a range comparable to that achieved in similar calculations of the more well understood core-level transition energies.

In Sec. II experimental procedures and reference-level methods are described, followed by presentation of the experimental results. A general model for interpreting AES spectra is then given which is applied to the ionic systems studied here. Section V compares the predicted and experimental spectra and discusses some implications of the agreement.

II. EXPERIMENTAL PROCEDURES

A. X-ray photoemission

The x-ray photoemission (XPS) data were obtained with a Hewlett-Packard 5950A ESCA spectrometer (hereafter referred to as the XPS system) using monochromatized Al $K\alpha$ x radiation. The samples were single crystals or thin polycrystalline films. The former, which were the same samples used in the Auger experiments, were cleaned by *in situ* heating to 200 °C. Carbon and oxygen contamination on these relatively inert crystals was essentially negligible ($\lesssim 0.5$ monolayer) as determined from analysis of their XPS core line spectra.

Thin films were prepared in the spectrometer sample chamber by evaporation of ultra pure NaF or MgF_2 crystallites onto polished copper substrates or by controlled oxidation of evaporated Al films. The spectra recorded from these samples were identical to those from the single crystals but were markedly more resolved due to the appreciable reduction in sample charging. This was also apparent in the binding energies in the single crystals which were observed to be 2–15 eV higher due to positive-charge accumulation. Sample charging appeared to be quite small for the thin films based on the observation of almost no binding-energy shift upon flooding the irradiated samples with low-energy electrons. However, this test in itself is not conclusive evidence of the absence of sample charging but is rather only an indication of its approximate order of magnitude. The fact that it is difficult to determine the level of charging with certainty in these insulators dictates the methods by which reference levels for their electron binding energies must be chosen. These procedures are discussed in Sec. II C.

B. Auger electron emission

The low-energy Auger transitions (kinetic energy <100 eV) were measured in a stainless-steel ultrahigh-vacuum system (hereafter referred to as the AES system) which has already been described.[5] Conventional ion- and liquid-nitrogen-temperature titanium sublimation pumping allowed a base pressure of less than 10^{-10} Torr, although most experiments were performed in the pressure range $(4-15)\times10^{-10}$ Torr. Single-crystal samples of NaF, MgF_2, and Al_2O_3 were mounted with high-purity indium "glue" on a molybdenum sample holder arm that was off axis and rotated in front of separate ports for each measurement. After heating to ~250–350 °C in ultrahigh vacuum for 5–10 min., a clear low-energy electron diffraction pattern was observed for each of the single-crystal surfaces. The absence of chemical impurities ($\lesssim 0.2$ monolayer) was determined by AES measurements which could be performed with normal incidence ($\varphi = 90°$) or oblique incidence ($\varphi = 20°$) using a PHI 10-234G single-pass cylindrical mirror-analyzer or a PHI 15-250 double-pass cylindrical mirror analyzer, respectively. Preliminary measurements indicated that radiation damage from the incident beam was severe for the normal incident beam, especially since a focused beam (~50-μm diameter) must be used. Therefore most AES measurements were performed with the double-pass analyzer using a defocused beam (~1-cm diameter) at the same total current $\sim10^{-5}$ A. The double-pass analyzer was operated in the retard mode at a constant resolution of 0.8 eV.

As previously reported for LiF and NaF,[6,7] we found that heating the crystals to 300–350 °C decreased the amount of charging due to the incident electron beam. Charging was further reduced in the AES measurements by adjusting the primary electron energy E_p to a value such that the secondary-emission coefficient was near unity, i.e., the sum of incident electron and emitted currents was minimized. Even with this procedure, however, charging effects were observed and these are discussed in more detail in Sec. II C.

Generally speaking, the charging effects were

most severe for Al_2O_3 in which the most detailed AES spectrum of the three crystals was observed. We therefore made a preliminary study of the oxide growth on aluminum metal. Metallic films of Al were prepared by *in situ* evaporation from 99.999% pure wire wound onto a tungsten filament. The films were deposited at room temperature on a polycrystalline molybdenum substrate and oxidized with dry O_2 gas from a high-purity flask admitted with standard leak valves. A total exposure of 300 langmuirs ($1\ L = 10^{-6}$ Torr sec) was sufficient to form a thin layer (~15 Å) of Al_2O_3 on the surface of the thick (~5000 Å) Al-metal film. This thin oxide layer is believed to be composed of small irregular patches overlaying the Al-metal substrate so that sample charging is assumed to be minimal.

High-energy Auger transitions (kinetic energy >1000 eV) were obtained with the XPS system using single crystals. The transitions, involving the decay of cation K holes by anion valence electrons, were sufficiently well defined above the secondary background so that signal differentiation was not required.

C. Reference energy levels

The reference energy used in most x-ray photoemission studies is the Fermi energy E_F. This is convenient for metals because the sample is in electrical equilibrium with the electron spectrometer (i.e., a common Fermi level) and the highest occupied energy level is E_F. For semiconductors and insulators two problems arise in trying to use E_F as a reference level.[8] The most obvious is that equilibrium may not be satisfied so that the sample and spectrometer Fermi levels differ by a charging potential. The second problem is that E_F is allowed to be at any position within the forbidden bandgap E_G. In particular, the position of E_F relative to the vacuum level E_{VAC} will be different for a thick insulator and for the *same* insulator in contact with a metal, i.e., a Schottky barrier will be established. This latter situation is often encountered in XPS experiments in which charging is minimized by either studying a thin layer of insulator such as a native oxide film or by vacuum deposition of a thin metallic film over a thick (bulk) insulating sample. For the samples studied in this work, the thick insulator case is applicable to the XPS system and the metal-insulator case is applicable to the AES system. A brief discussion of these two situations, which are so frequently encountered in many other XPS and AES experiments, is worthwhile at this point. In what follows we make use of the concept of "local" equilibrium so that the values of E_G, E_{VAC}, and E_F remain well-defined quantities. This will be true even in the presence of a charging shift since the total number of electrons per atom remains essentially unchanged.

The schematic energy-level diagram for a thick insulator is shown in Fig. 1(a). The Fermi level is located in the middle of the bandgap and the sample work function, φ_{sa}, is given in terms of the photoelectric threshold, Φ_I,

$$\varphi_{sa} = \Phi_I - \tfrac{1}{2}E_G \ . \tag{2.1}$$

This location of E_F is determined by the equilibrium of charge flow between the conduction and valence bands, i.e., for every electron thermally excited from the valence to conduction band there must be a hole excited from the conduction to valence band. For the case of a thick insulator this is the only mechanism of maintaining equilibrium. However, this is not true for the case of a metal in contact with the irradiated insulator as shown in Fig. 1(b). Now to maintain equilibrium the metal provides an additional source of electrons and holes and a contact potential develops across the insulator. Figure 1(b) shows an "ideal" metal-insulator contact[9] where the potential, and hence the work function, at the metal-insulator interface is determined entirely by the

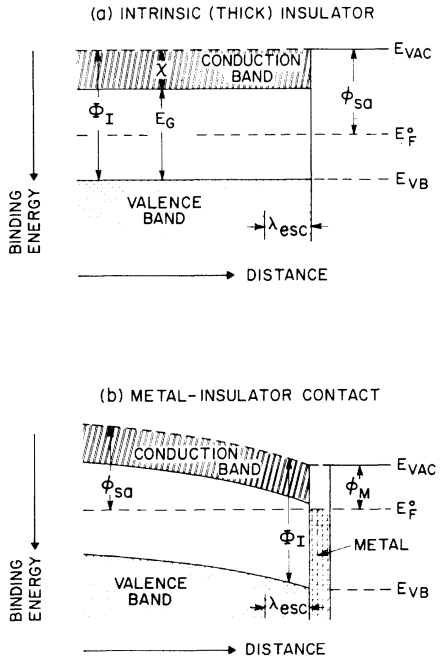

FIG. 1. Energy-level diagrams for (a) intrinsic insulators showing quasi-Fermi level near the center of the forbidden gap and for (b) a metal-insulator contact in the usual Schottky limit of no interface states. For the latter case the Fermi level is determined by the metal and not by the insulator.

metal. The more typical intermediate case involving interface states or traps was first discussed by Bardeen.[10] However, in this work we consider only the two extremes shown in Fig. 1 because of their applicability to the samples studied in our experiments. From Fig. 1(b) it is clear that the work function of the metal-insulator system is equal to that of the metal φ_M and not of the insulator. Since the electron escape depth λ_{esc} is very short (~20 Å) compared to the total band-bending distance (~10^4 Å) as shown in Fig. 1(b), one expects to measure well-defined energy levels which are not broadened by the spatial variation shown. For example, the absolute energy of the valence-band edge E_{VB} is essentially constant over λ_{esc} and is given by

$$E_{VB} = E_{VAC} - \Phi_I \ , \tag{2.2}$$

where the photoelectric threshold Φ_I remains unchanged. This "ideal" contact behavior has been verified by electrical tunneling measurements for a large number of insulators and large bandgap semiconductors[11] and so is expected to apply to the ionic compounds studied in this work.

From the above considerations we see that for a fixed level of radiation on a given (thick) insulator the degree of charging and the vacuum level position are significantly influenced by the presence of a metal overlayer. With regards to our particular experiments, the samples irradiated with electrons in the AES system had metal-insulator contacts while those irradiated with photons in the XPS system did not; the zero-kinetic-energy reference levels in the two systems are therefore distinctly different. It is necessary to choose a common and experimentally accessible reference level in order to compare electron energies from one system with another. We have chosen the vacuum level of the clean, bulk insulator in the XPS system as the common reference level, although the valence band edge could have also been used.[12] Electron kinetic energies in the XPS system relative to the vacuum level E_k^V are related to the binding energies relative to the valence band edge E_B^{VB} by the equation

$$E_k^V = \hbar\omega - E_B^{VB} - \Phi_I \ , \tag{2.3}$$

where $\hbar\omega$ is the Al $K\alpha$ photon energy. The photoelectric threshold values are obtained from optical absorption[13,14] and photoemission data.[15,16] The electron kinetic energies from samples in the AES system are then referenced to the corresponding vacuum levels of those samples in the XPS system through measurement of core-level transitions common to both systems. For example, if the kinetic energy of the O($KL_{2,3}L_{2,3}$, ^1D) transition in Al_2O_3 measured with the XPS system is E_1 and the corresponding energy measured with the AES system is E_2, then the correction factor due to charging and vacuum level differences (which is thus common to all the Auger transition energies measured in the AES system) is simply $\Delta = E_1 - E_2$. This factor, determined from Na, Mg, F, and O KLL transitions in the various samples, was 1 – 2 eV. The largest source of experimental uncertainty in these measurements arose from electron beam-induced defect states in the samples which affected their charging potentials and hence the precision of the measured correction factor. This uncertainty of approximately ±1.5 eV is thus a limiting factor in the comparison between theoretically predicted and experimentally measured Auger energies.

III. EXPERIMENTAL RESULTS

A. X-ray photoemission

Experimental results for the x-ray photoemission spectra of Al_2O_3, MgF_2, and NaF are shown in Fig. 2. The samples were the single crystals also used in the Auger measurements. The binding-energy reference in Fig. 2 is the valence-band maximum, determined by a linear extrapolation of the leading valence band edge at half-intensity. The detailed valence-band features have not been interpreted since only a quasiatomic picture was used to interpret the interatomic Auger transitions. To obtain the binding energies relative to the vacuum level one must add the photoelectric threshold energies Φ_I[13-16,17] (see Fig. 1 and Sec. II C). The numerical values so obtained are given in Table I along with similar values obtained on thin-film samples that have been referenced to the quasi-Fermi level. It is important to note that on the thin-film samples with essentially little or no charging the quasi-Fermi level is found to be within—but not at the center—of the energy gap. This serves to illustrate the hazards in attempting to use a "Fermi-level" reference for insulating materials even in thin-film form.

The x-ray photoemission results for NaF in both the single crystal and thin-film forms are shown in Fig. 3. Comparison of the two spectra dramatically demonstrates the broadening effect of inhomogeneous sample charging in the single crystal. Similar effects were seen for Al_2O_3 and MgF_2. Since such broadening affects the position of the core level peaks relative to the extrapolated *edge* of the (broadened vs unbroadened) valence band, it is important to minimize sample charging even when determining *relative* binding energies in insulators.

B. Auger

Low-energy Auger electron spectra are shown in Fig. 4 for a clean Al metal film and one after exposures of 10, 100, and 300 L of O_2 gas (1 L $= 10^{-6}$ Torr sec). The data were recorded as the negative second derivative of the electron energy distribution in order to suppress the rapidly varying true secondary background signal. This al-

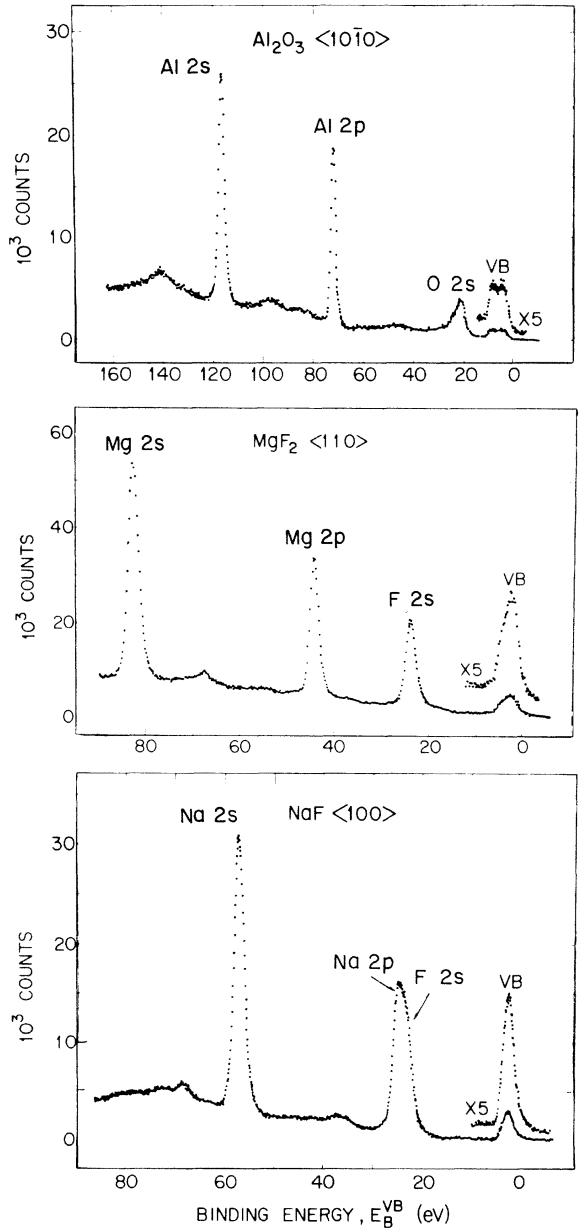

FIG. 2. X-ray photoemission spectra of Al_2O_3, MgF_2, and NaF showing the valence band and shallow core levels which participate in low-energy interatomic Auger processes. Binding energies are shown referenced to the valence band edge.

TABLE I. Summary of XPS binding energies (in eV).

Compound	Level	$E_B^{"F"}$ [a]	E_B^{VB} [b]	E_B^{V} [c]
Al_2O_3	VB	9.2	5.5	16.0
	O 2*s*	24.2	20.5	31.0
	Al 2*p*	75.4	71.4	81.9
	Al 2*s*	120.2	116.2	126.7
MgF_2	VB	12.1	3.4	14.4
	F 2*s*	32.9	24.2	35.2
	Mg 2*p*	53.5	44.8	55.8
	Mg 2*s*	92.2	84.5	95.5
NaF	VB	8.8	1.9	13.4
	F 2*s*	29.3	22.4	33.9
	Na 2*p*	31.1	24.2	35.7
	Na 2*s*	63.8	56.9	68.4

[a] Referenced to the quasi-Fermi level. See text for details.
[b] Referenced to the top of the valence band.
[c] Referenced to the vacuum level of the bulk crystal. See text for details.

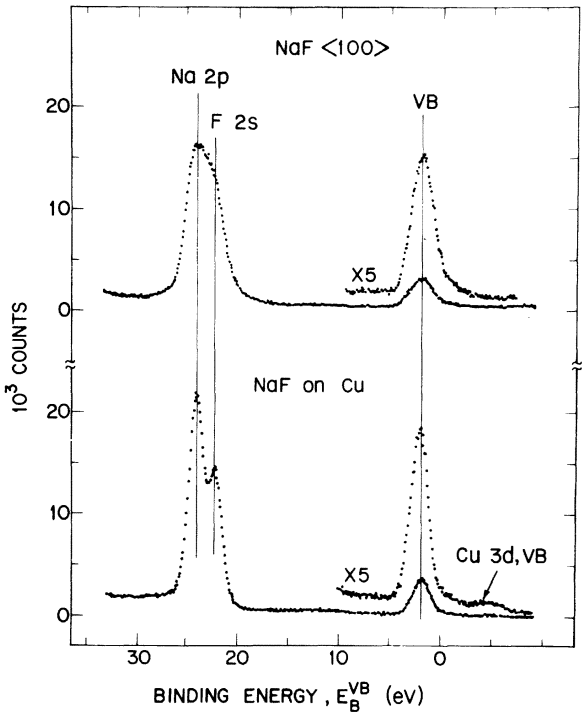

FIG. 3. X-ray photoemission spectra of NaF showing the valence band and shallow core levels for a single crystal (upper) and for a thin film evaporated onto a copper substrate (lower). The evaporated film is more resolved due to reduced inhomogeneous broadening from charging and is thus more reliable for determining core-level binding energy-*peak* positions relative to an (unbroadened) valence band *edge*.

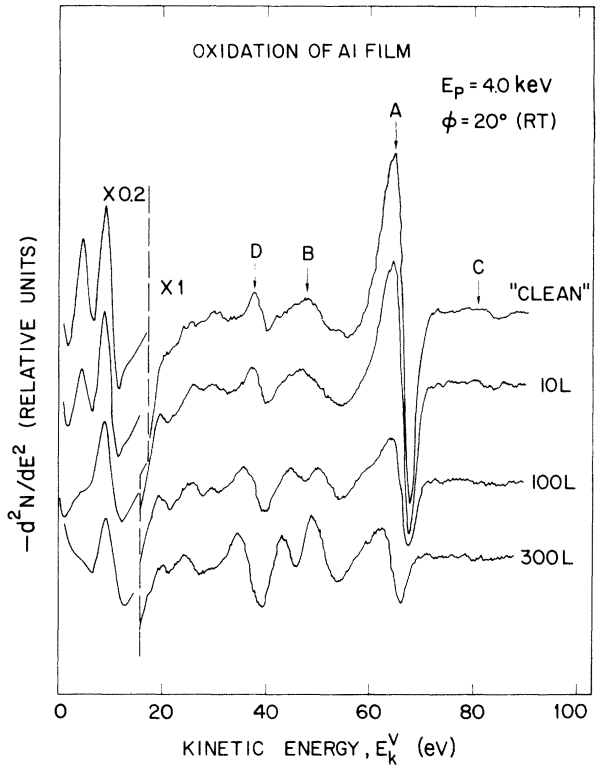

FIG. 4. Low-energy Auger electron spectra showing the oxidation of an aluminum film. The gas exposures of O_2 in langmuirs (1 L = 10^{-6} Torr sec) are given for each curve. General peak assignments are given in Table II. Kinetic energies are referenced to the vacuum level of bulk Al_2O_3.

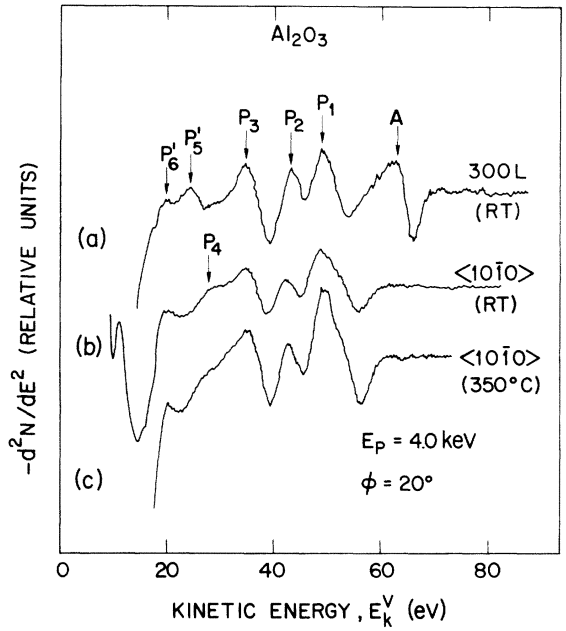

FIG. 5. Low-energy Auger electron spectra for Al_2O_3 from a 300-L oxidized Al film and from a bulk crystal. General peak assignments are given in Table II. Kinetic energies are referenced to the vacuum level of bulk Al_2O_3.

lowed a clear observation of secondary electron threshold structure at kinetic energies of 11 and 6.5 eV above the vacuum level of the clean metal. These are identified as thresholds for the bulk plasmon and surface plasmon, respectively, of Al metal.[18] The energies obtained by adding the work function $\varphi_M = 4.2$ eV are 15.2 and 10.7 eV, in excellent agreement with the corresponding energies obtained by electron energy loss[19] and x-ray photoemission measurements.[20] The other features labeled *A* and *B* are identified as $L_{2,3}VV$ transitions and its plasmon satellite, respectively. The weak feature *C* is the double ionization transition $L_{2,3}VV$ while peak *D* is the $L_1L_{2,3}V$ transition.

With increasing oxygen exposure the Al-metal Auger transitions become weaker, the surface/bulk plasmon threshold peak ratio decreases, and additional transitions appear due to a film of Al_2O_3. The possibility of an intermediate interfacial oxide compound of unknown composition cannot be completely eliminated at this point but will be discussed further in Sec. V. Most of the peaks observed in the thin-film data are, however, also found for bulk single crystals of Al_2O_3 as shown in Fig. 5.

The kinetic scale is referenced to the vacuum level of the bulk Al_2O_3 crystal using procedures described in Sec. IIC. Aligning peak P_1 from the thin-film results with that obtained from the bulk results, curves (*b*) and (*c*), also aligns peaks P_2 and P_3, as well as approximately aligning the true secondary peak (not shown). The bulk-crystal measurements shown in Fig. 5 were obtained at room temperature and at an elevated temperature of about 350 °C. Upon heating, the secondary electron-emission coefficient was reduced, which resulted in a decrease in charging from about +6 to +2 eV. Peak P_4 is observed on top of a rapidly varying secondary electron background that even the second derivative cannot entirely suppress, and so its exact position is not very well defined. Peak P_5' is clearly observable only in the thin-film measurements while P_6' is seen in both the thin-film and bulk experiments. The former peak may be an interatomic transition which is obscured by the background in the bulk measurements; the latter peak's identification is not well established. The uncertainty in the assignments for these peaks is indicated by the prime notation.

Figure 6 shows similar low-energy Auger results for single-crystal MgF_2. The electron beam produced some decomposition and resulted in a superimposed Mg-metal spectrum with peaks labeled *A*, *B*, and *C*. The decomposition (and Mg-

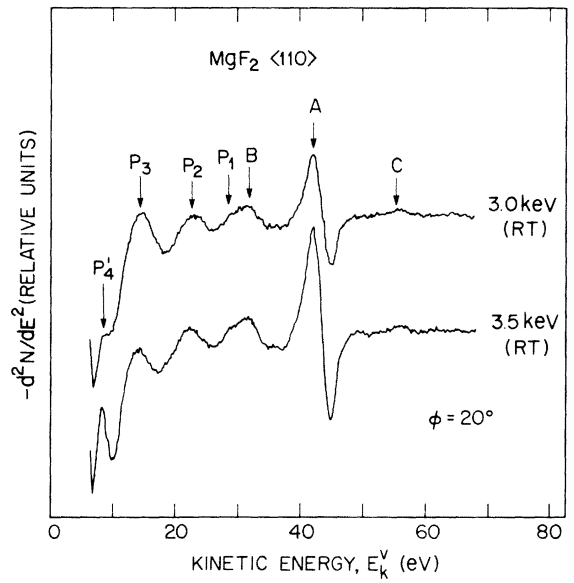

FIG. 6. Low-energy Auger electron spectra from MgF_2 crystal with some Mg metal due to electron-beam decomposition. General peak assignments are given in Table II. Kinetic energies are referenced to the vacuum level of bulk MgF_2.

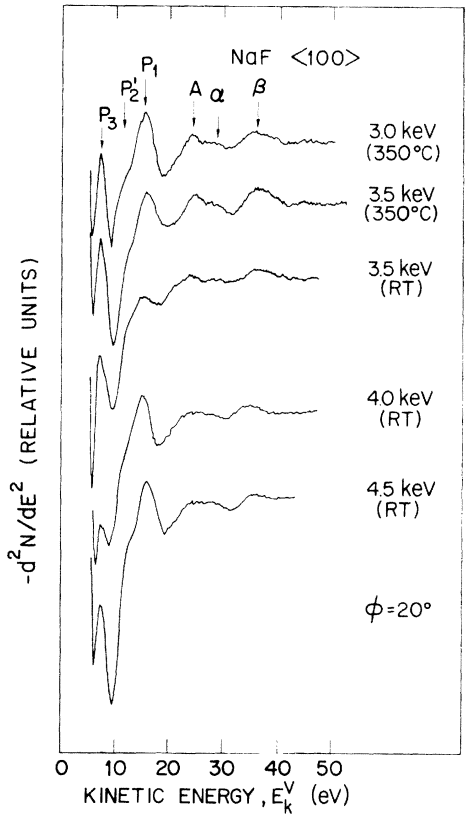

FIG. 7. Low-energy Auger electron spectra for NaF under several different experimental conditions to establish intrinsic transitions of NaF and extrinsic features from Na metal and color centers. General peak assignments are given in Table II. Kinetic energies are referenced to the vacuum level of bulk NaF.

metal peak height) was approximately a factor of two smaller with the grazing-incidence gun than with the normal-incidence gun. The peak assignments for *A*, *B*, and *C* are the same as for Al metal given above. The Auger transition of MgF_2 labeled P_1 is overlapped by the $L_1L_{2,3}V$ transition of Mg metal and so it is difficult to establish its position precisely. The peaks labeled P_2 and P_3 are clearly identified as interatomic transitions but P_4' may arise from other origins. These will be discussed further in Sec. V.

The low-energy Auger data for NaF are shown in Fig. 7 for several different excitation energies and both room temperature and $T \approx 350\,^{\circ}C$. These various conditions were used in order to vary the true secondary electron background since the small XPS binding energies of NaF imply small kinetic energies in the Auger spectra of this compound. We also observed an electron-beam-induced Na-metal peak indicated by *A*. As observed for LiF,[21,22] higher-energy transitions labeled α and β are apparent and are likely due to color centers or other defects. The peaks labeled P_1 and P_3 are identified as interatomic Auger transitions. The position and intensity of P_2' are difficult to establish since it lies on a rapidly changing background. Possible sources for its origin are discussed in Sec. V.

The high-energy Auger data for MgF_2 and NaF taken with the XPS system are shown in Fig. 8 (the Al Kα exciting radiation precluded study of analogous transitions in Al_2O_3). Although the interatomic Auger transitions are significantly weaker than the intra-atomic $KL_{2,3}L_{2,3}(^1D)$ transitions for Na and Mg, it is possible to identify the former transitions without the need for signal differentiation. The extreme weakness of the peaks in MgF_2, however, precludes observation of all the expected transitions due to interference with a C 1*s* signal coming from very small amounts of surface contamination.

A summary of the peak positions observed for Al_2O_3, MgF_2, and NaF crystals is given in Table II. As mentioned above, all the peak energies are referenced to the vacuum level of the bulk crystals.[23]

IV. THEORETICAL MODEL

This section is divided into several parts. In part A, a qualitative framework is given for evaluating Auger electron energies and transition

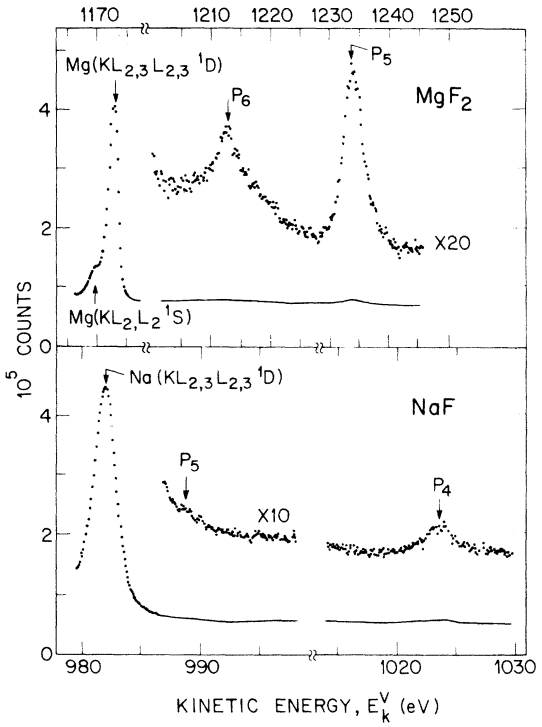

FIG. 8. High-energy Auger electron spectra for MgF_2 and NaF, showing very weak interatomic transitions. The intra-atomic Na and Mg $KL_{2,3}L_{2,3}$, ^1D transitions are also shown for comparison. The kinetic energies are referenced to the vacuum levels of the bulk crystals.

TABLE II. Summary of AES peak positions (in eV) and assignments. [a]

Compound	E_K^V	Label	Assignment
	80	C	Al double ionization
	64	A	Al metal $L_{2,3}VV$
	49	B	Al bulk plasmon loss
	37	D	Al metal $L_1L_{2,3}V$
	49.0	P_1	Interatomic
	42.0	P_2	Interatomic
Al_2O_3	34.5	P_3	Interatomic
	27.4	P_4	Interatomic
	24.1	P_5	Interatomic
	19.6	P_6'	•••
	56	C	Mg double ionization
	42	A	Mg metal $L_{2,3}VV$
	32	B	Mg bulk plasmon loss
MgF_2	28.2	P_1	Interatomic
	22.5	P_2	Interatomic
	14.4	P_3	Interatomic
	8.3	P_4'	•••
	1234.1	P_5	Interatomic
	1212.9	P_6	Interatomic
	24	A	Na metal $L_{2,3}VV$
	16.0	P_1	Interatomic
NaF	13.0	P_2'	•••
	7.0	P_3	Interatomic
	1023.4	P_4	Interatomic
	(991)	P_5	Interatomic

[a] Referenced to the vacuum level of the bulk crystals.

rates in solid-state systems. Its various subsections ultimately describe how energies and intensities of interatomic Auger transitions may be determined or inferred from empirical and theoretical approaches. Part B applies the methods and concepts of part A to the specific examples that have been studied in the present work.

A. General

1. Auger energies

In an XYZ Auger transition, a hole in level X decays by annihilation with a lesser bound electron from level Y, and an electron from level Z is simultaneously ejected into the continuum. The ejected electron is termed the XYZ electron and its kinetic energy is called the Auger energy.[1] Although similar treatments have been previously described for intra-atomic Auger energies,[24-26] a systematic approach for calculating Auger energies is presented here to gain insight into the procedures for evaluating energies of interatomic transitions.

The factors determining a typical intra-atomic Auger energy are considered for the exemplary case of the ^1D multiplet state of the KLL manifold in neon. The Ne $(KL_2L_3, {}^1D)$ energy is given by

$$E_k^V(KL_2L_3, {}^1D) = E_B^V(K) - E_B^V(L_2L_3, {}^1D), \qquad (4.1)$$

where E_B denotes the binding energy of the initial singly ionized K or final doubly ionized L_2L_3 state. The superscript denotes the vacuum reference level common to all quantities. (As a point of clarification, only absolute magnitudes of energies are used; sign changes are made explicitly.) Since it is difficult to calculate the double hole-state energy $E_k^V(KL_2L_3)$ directly, one-hole (one-electron) calculations are used with corrections to these energies added on separately. Denoting Hartree-Fock (Koopmans's theorem) energies by ϵ, Eq. (4.1) can be rewritten by

$$E_k^V(KL_2L_3, {}^1D) = \epsilon^V(K) - \epsilon^V(L_2) - \epsilon^V(L_3) - u_i(L_2L_3, {}^1D) - P_i(K) + P_i(L_2) + P_i(L_3) + P_{ic}(L_2L_3) + \Delta\epsilon_{\text{rel}} + \Delta\epsilon_{\text{corr}} . \qquad (4.2)$$

Here $u_i(L_2L_3)$ is the repulsive intra-atomic hole-hole interaction energy, and $\Delta\epsilon_{\text{rel}}$ and $\Delta\epsilon_{\text{corr}}$ are the changes between initial- and final-state relativistic and correlation energies, respectively. For our purposes these latter terms shall be ignored because they will be implicitly included

later using empirically determined energies. More will be said about u_i further on.

The term $P_i(X)$ is the difference between the Koopmans's theorem energy and the self-consistent Hartree-Fock energy of the X hole state and represents the intra-atomic polarization energy of the electrons surrounding the X hole.[27,28] Its origin may be physically understood from the purely classical view whereby a test charge (core hole) induces a screening cloud of radius r; the energy for this is simply $(ze)^2/2r$, where here $z=1$. By energy conservation, the outgoing electron has a binding energy lower by an amount identical to that gained by having its screened from the hole.

To understand the P_{ic} term in Eq. (4.2), consider two holes Y and Z which interact with their own screening clouds to give polarization energies $e^2/2r_Y$ and $e^2/2r_Z$, respectively. If the holes are separated by an average screening length r_{YZ} such that they also interact with each other's screening cloud, the total intra-atomic polarization energy of the double hole-state $P_i(YZ)$ is then

$$P_i(YZ)=\frac{e^2}{2}\left(\frac{1}{r_Y}+\frac{1}{r_Z}+\frac{2}{r_{YZ}}\right). \tag{4.3}$$

The first two terms are just the single-hole polarization energies $P_i(Y)$ and $P_i(Z)$ in Eq. (4.2); the third term represents what we shall refer to as an intra-atomic *cross* polarization energy, $P_{ic}(YZ)$.[29] It is obviously the magnitude of this term [along with $u_i(YZ)$] that distinguishes between a double single-hole or single double-hole-state calculation.

Methods for accurately and explicitly calculating $P_{ic}(YZ)$ do not exist at present so approximations must be used. Recently, Shirley[30] has extended the method of Hedin and Johannson[28] (which calculates single-hole polarization energies) to the case of double holes in KL_1L_1 transitions, and finds in that case that to a first approximation

$$P_{ic}(L_1L_1)\cong 2P_i(L_1). \tag{4.4}$$

Classically this is equivalent to assuming that two singly charged holes X and X' can be approximated by a single doubly charged hole XX', so that $r_X = r_{X'} \cong r_{XX'}$ and Eq. (4.3) reduces to

$$P_i(XX')\cong P_i(2X)=\tfrac{1}{2}e^2(4/r_X). \tag{4.5}$$

This approximation is valid if core electrons X and X' are sufficiently similar such that each contributes only a fractional polarization energy to the other's hole production. In the particular case of KL_1L_1 transitions in an $n=2$ closed shell atom, each L_1 electron can be assumed to contribute $\sim\frac{1}{8}$ of the polarization energy arising from $n=2$ electrons, so differences between $\frac{7}{8}$ or $\frac{3}{4}$ of the $n=2$ "intrashell" polarization energy are presumed to be small.[31] This approximation, Eq. (4.5), will be seen to be useful in our analysis of interatomic transition energies.

So far polarization energies have only been discussed for isolated atoms. If the atoms are in a polarizable medium, such as a molecule or solid, additional energy is gained upon hole formation. Various methods exist for calculating the additional polarization energy (also called extra-atomic relaxation energy), with varying degrees of accuracy, sophistication, and applicability.[32] For the case of the ionic compounds investigated in this work we use the method of Mott and Littleton,[33] which has been used previously to interpret XPS spectra of alkali halides.[8] Although the method has only been applied to crystals with[8,33] NaCl and[8] CsCl structures, the feature of rather localized electrons and consequently small polarization energies in ionic crystals (i.e., small relative to metals) enables these energies to be approximated in other, more complicated ionic crystals without introducing sizeable errors.

The additional extra-atomic polarization energy P_x modifies the Auger energy given by Eq. (4.2) for a free atom. Using the $Na^+(KL_2L_3,{}^1D)$ transition in NaCl as an appropriate analog to the neon atom, Eq. (4.2) is now given by

$$\begin{aligned}E_k^V(KL_2L_3,{}^1D)=\epsilon^V(K)-\epsilon^V(L_2)-\epsilon^V(L_3)-u_i(L_2L_3,{}^1D)\\ -[P_i(K)+P_x(K)]+[P_i(L_2)+P_x(L_2)]\\ +[P_i(L_3)+P_x(L_3)]\\ +[P_{ic}(L_2L_3)+P_{xc}(L_2L_3)].\end{aligned} \tag{4.6}$$

The term $P_{xc}(L_2L_3)$ shall be called an extra-atomic *cross* polarization energy[34]; its origin is completely analogous to the intra-atomic P_{ic} in Eq. (4.3). It is obvious from analogy with Eq. (4.4) that $P_{xc}(L_2L_3)$ can be approximated by

$$P_{xc}(L_2L_3)\cong 2P_x(L_2)=2P_x(L_3). \tag{4.7}$$

The validity of this approximation is on rather firm ground because the absence or presence of an additional intra-atomic core hole has virtually no effect on the single-hole polarization of the electrons that are extra-atomic in nature, i.e., of which the *additional* intra-atomic hole is not a part. We see that using Eq. (4.7) and the Mott and Littleton theory for calculating one-electron extra-atomic polarization energies, it is possible to readily calculate extra-atomic cross-polarization energies.

In discussing the repulsive hole-hole energy u, as in the case of polarization energies it is necessary to specify whether the two holes are on the same or different atomic sites. Up until now the repulsive energy has been denoted by u_i implying

a localized nature for intra-atomic holes. If the holes are separated in a crystal, for example, the repulsive energy is given by u_x, where x denotes the nonlocalized nature of the holes. Two holes Y and Z on isolated atoms separated by a distance R_{YZ} (note the distinction from r_{YZ}, which is an average screening radius) experience a repulsive hole-hole energy

$$u_x(YZ) = e^2/R_{YZ} \ . \tag{4.8}$$

If the different atomic sites are in a polarizable medium, e.g., a crystal, their *net* repulsive energies will be modified (reduced) by the extra-atomic cross-polarization energy discussed above, giving a *total nonlocalized* hole-hole interaction energy

$$U_x(YZ) = u_x(YZ) - P_{xc}(YZ). \tag{4.9}$$

From Eqs. (4.3), (4.5), and (4.8) this is given classically by

$$U_x(YZ) = e^2/R_{YZ} - \tfrac{1}{2}e^2(2/r_{YZ}) \ . \tag{4.10}$$

The total nonlocalized hole-hole energy may also be written

$$U_x(YZ) \cong e^2/R_{YZ}\epsilon_\infty \ , \tag{4.11}$$

where ϵ_∞ is the high-frequency dielectric constant; the extra-atomic cross-polarization energy is then given by

$$P_{xc}(YZ) \cong (e^2/R_{YZ})(1 - 1/\epsilon_\infty) \ . \tag{4.12}$$

Equation (4.12) is by definition only approximate because of the average screening distance used and the assumed average dielectric response acting over that distance. Nevertheless, for the case of separated holes in a polarizable medium it offers a simple, empirical, and physically reasonable approach for estimating the total nonlocalized hole-hole interaction energy.

If the holes are localized on the same atomic site, regardless of its environment the above classical approach is no longer valid. Equations (4.8)–(4.12) implicitly ignore the correlated motion of the Fermi holes which give rise to various multiplet configurations. The localized hole-hole interaction energy $u_i(YZ)$ may, in principle, be calculated for each multiplet state using the intermediate coupling theory of Asaad and Burhop.[35] However, we shall ultimately need the *total localized* hole-hole interaction energy $U_i(YZ)$ and this involves a separate calculation for the intra-atomic cross-polarization energy $P_{ic}(YZ)$, i.e.,

$$U_i(YZ) = u_i(YZ) - P_{ic}(YZ) \ . \tag{4.13}$$

Rather than calculating $u_i(YZ)$ and $P_{ic}(YZ)$ separately, we instead use an empirical approach as was done for the nonlocalized hole case above.

A prescription for empirically determining $U_i(YZ)$ may be seen for the case of the KL_2L_3, ^1D transition in neon. The double hole-state energy of the ^1D configuration is obtained from optical data for the Ne III ($Ne\ 2s^2p^4$) state and is 65.83 eV.[36] [Using this value, Eq. (4.1), and the XPS value for the Ne 1s binding energy of 870.37 eV,[37] one obtains an Auger energy of 804.54 eV, in good agreement with the measured value of 804.15 ± 0.40 eV.[38]] It follows that knowledge of $E_B^V(L_2L_3, {}^1D)$ and empirical values for the individual single hole-state energies $E_B^V(L_2)$ and $E_B^V(L_3)$ enables the determination of the total intra-atomic hole-hole interaction energy by

$$U_i(L_2L_3, {}^1D) = E_B^V(L_2L_3, {}^1D) - E_B^V(L_2) - E_B^V(L_3) \ . \tag{4.14}$$

The advantage of using empirical data is obvious since all intra-atomic polarization, correlation, relativistic, and hole-hole interaction energies are implicitly included. As was pointed out, however, it is usually not possible to measure double hole-state energies directly, and this is especially true in solid-state systems. The next best approach is to use empirically determined one-electron energies, $E_B(X)$, which are much more readily accessible from XPS. Returning to the case of $Na^+(KL_2L_3, {}^1D)$ Auger electrons from NaCl, Eq. (4.6) may be rewritten in terms of one-electron binding energies by

$$E_k^V(KL_2L_3) = E_B^V(K) - E_B^V(L_2) - E_B^V(L_3) - u_i(L_2L_3) + [P_{ic}(L_2L_3) + P_{xc}(L_2L_3)] \ . \tag{4.15}$$

Note that a common vacuum reference level has been used for all quantities. If optical data exist for the multiplet state under consideration, substitution of Eq. (4.13) into Eq. (4.15) gives the general expression for an XYZ Auger electron from an atom or ion in a solid in terms of empirical one-electron binding energies:

$$E_k^V(XYZ) = E_B^V(X) - E_B^V(Y) - E_B^V(Z) - U_i(YZ) + P_{xc}(YZ). \tag{4.16}$$

For atoms or ions where optical data exist the only quantity that must be calculated is the extra-atomic cross-polarization energy $P_{xc}(YZ)$.

The form of Eq. (4.16) makes clear why chemical shifts in intra-atomic Auger spectra are usually so much larger between metals and their compounds than corresponding chemical shifts observed in XPS. The first three terms incorporate the XPS chemical shifts while the $U_i(YZ)$ term, being intra-atomic, is invariant to the chemical environment. Therefore the last term, the extra-

atomic cross polarization energy, is seen to be responsible.[24,26] It is easily understood to be larger in metals than in nonmetals because of the metal's significantly larger electronic polarizability.

We conclude this section on Auger energies by considering the situation with which the present work is principally concerned, namely, Auger transitions involving electrons from neighboring sites. In these cases it is again important to specify the localized or nonlocalized nature of the final-state holes, and this depends on the particular transitions involved. These transitions will be discussed further in Sec. IV A 2, but for now we simply prescribe methods for calculating their energies. If the final-state double holes are localized on the same nearest-neighbor site, Eq. (4.16) applies with the last four terms being appropriate to the nearest neighbor. If the holes are nonlocalized on different nearest-neighbor sites, the $U_i(YZ)$ term is clearly no longer applicable. In this case we have shown that it is appropriate to use $U_x(YZ)$, which implicitly includes $P_{xc}(YZ)$ [(Eq. (4.9)]. Upon substitution of Eq. (4.11) into Eq. (4.10) and elimination of the additional $P_{xc}(YZ)$ term to avoid double counting we get

$$E_k^V(XYZ) = E_B^V(X) - E_B^V(Y) - E_B^V(Z) - e^2/R_{YZ}\epsilon_\infty . \tag{4.17}$$

The final interatomic transition that is possible involves nonlocalized holes with one hole on the initial hole-state site and the other on a nearest-neighbor site. In this case Eq. (4.17) applies but the effective distance between the two holes R_{YZ} is now different.

We summarize this section by listing the expressions for calculating Auger energies from empirical one-electron binding energies:

$$E_k^V(XYZ) = E_B^V(X) - E_B^V(Y) - E_B^V(Z) + \cdots ,$$

(a) $-U_i(YZ) \equiv -u_i(YZ) + P_{ic}(YZ)$, localized holes in an atom;

(b) $-u_x(YZ)$, nonlocalized holes in different atoms;

(c) $-U_i(YZ) + P_{xc}(YZ)$, localized holes in a solid;

(d) $-U_x(YZ) \equiv -u_x(YZ) + P_{xc}(YZ)$, nonlocalized holes in a solid.

2. *Auger intensities*

Using time-dependent first-order perturbation theory Wentzel[39] first calculated Auger transition probabilities assuming the time-independent perturbation to be the Coulombic interaction between the bound annihilating and ejected electrons in the presence of a core vacancy. Denoting the initial hole-state wave function as φ, the continuum wave function of the ejected Auger electron as ψ, and the bound states of the annihilating and ejected electrons as Φ and Φ', respectively, the transition probability is proportional to the square of the matrix element

$$\langle \varphi(1)\psi(2) \left| e^2/|\vec{r}_1 - \vec{r}_2| \right| \Phi(1)\Phi'(2) \rangle , \tag{4.18}$$

where the indistinguishability of electrons 1 and 2 has been ignored for simplicity. The expansion and separation of the matrix element into angular and radial factors is straightforward assuming the wave functions φ, Φ, and Φ' are on the same site, i.e., in the same central field. In this intra-atomic situation it follows that Auger probabilities depend most strongly on the radial overlap of wave functions $\varphi(1)$ with $\Phi(1)$ and $\psi(2)$ with $\Phi(2)$. With this simple guideline a qualitative assessment of relative Auger rates for a given core-hole state is possible.

The above considerations refer to purely intra-atomic transitions in which the *sites* of initial singly ionized and final doubly ionized states are identical. This is not the case in situations where nonradiative decay of least-bound core holes by intra-atomic electrons is either energetically forbidden or improbable due to small electron overlap with the initial hole-state. In such cases it is necessary to consider hole decay from those electrons that are both spatially and energetically favorable, viz., the valence electrons of the neighboring atoms. Allowing for these interatomic transitions, a more general expression for the Auger transition matrix may be written

$$\langle \varphi_A(1)\psi(2) \left| e^2/|\vec{r}_1 - \vec{r}_2| \right| \Phi_{A,B}(1)\Phi'_{A,B}(2) \rangle , \tag{4.19}$$

where the initial hole-state site has been denoted by the subscript A and the nearest-neighbor sites to it denoted by B. Analogous to the intra-atomic case, the matrix element involving different atomic sites may also be expanded into angular and radial components, but here the symmetry of the nearest-neighbor distribution must be taken into account. Abundant calculations for intra-atomic transitions exist in the literature,[4] but no attempts so far have been made to calculate interatomic transition probabilities.[40] In the absence of such

calculations, a discussion of expected interatomic Auger line intensities must proceed along lines of intuition and plausibility.

With this qualification and the above considerations of spatial overlap, we classify interatomic Auger transitions in the following way. The distinction between inter- and intra-atomic XYZ processes is made by the notations[3]

$A(X)A(Y)A(Z)$ or AA,

$A(X)B(Y)B(Z)$ or BB,

$A(X)A(Y)B(Z)$ or AB.

The first process corresponds to the case in which all levels are associated with the initial hole site A and is thus the conventional intra-atomic process, abbreviated as AA. The BB mechanism then describes the "pure" interatomic picture. The AB process is a "mixed" transition but will still be referred to as interatomic. It will be seen in Sec. IV B that the AB mechanism usually represents an interatomic Coster-Kronig process, the generic term describing nonradiative hole annihilation by an electron within the same principal quantum shell. We have not listed the BA process, which may be regarded as the exchange analog of the "direct" AB process, on the grounds that the probability for its occurrence is extremely small with respect to the other mechanisms.

A final type of interatomic Auger process involves hole filling and electron ejection from nearest-neighbor valence electrons, but the final-state double holes are sufficiently nonlocalized such that they may be regarded as single holes.[21] This criterion has been discussed above whereby Eq. (4.17) is appropriate for calculating the Auger energies. This type of transition is referred to in our notation by

$A(X)B(Y)B(Z)'$ or BB'.

It is tempting to think of the BB' transitions as involving two distinct nearest-neighbor sites; in calculating the repulsive interaction with each other using Eq. (4.8) we have in fact assumed them to be separated by effective distances appropriate to this model. However, it should be pointed out that in distinguishing between localized holes in BB mechanisms and nonlocalized holes in BB' mechanisms this picture is unnecessary. In fact, the picture of hard ionic spheres may emerge from the distinct-site model and this should be avoided. Valence electrons, no matter how localized in an ionic crystal, are delocalized in a valence band spanning the entire lattice. This delocalization is actually essential because without it interatomic-transition probabilities would be zero due to the nonoverlap of valence wave functions $\Phi_B(1)$ with $\varphi_A(1)$ in Eq. (4.19). Therefore, while we shall discuss nearest-neighbor valence electrons as being associated with atomic sites as such, it should be borne in mind that these wave functions are most definitely extended. Treating the relatively narrow valence bands as semilocalized in ionic compounds is devised purely for computational convenience.

B. Calculation of interatomic Auger energies

In this section the methods of the previous section along with the empirical binding energies of Sec. III are used in the calculations of interatomic Auger energies. As an illustrative example we consider Al_2O_3. Extensions of our methods to other crystals are straightforward.

Before calculating their energies, it is necessary to determine when the interatomic process will occur, i.e., under what circumstances they compete with intra-atomic transitions. In Al_2O_3, an initial-state Al hole can be formed in either the K, L_1, or $L_{2,3}$ level. Holes in the M_1 and $M_{2,3}$ levels of Al in Al_2O_3 can be neglected since they have been essentially removed into the valence band primarily composed of oxygen $L_{2,3}$ electrons. An Al(K) hole bound by about 1.5 keV decays almost exclusively via nonradiative transitions, and of those the intra-atomic KLL transitions are most important.[1,4] In the notation from the above section, these are denoted by Al(K)Al(L)Al(L) or AA. The reason for their predominance over possible interatomic transitions, e.g., Al(K)O(L)O(L), follows from Eq. (4.19): The tightly bound Al(K) hole overlaps much more strongly with the localized Al(L) electrons than with the comparatively more delocalized and removed oxygen valence electrons.

An initial vacancy in the Al($L_{2,3}$) level is quite different from the Al(K) hole case since the lesser-bound electrons capable of filling it are in the oxygen-derived valence band. In the first level of approximation an average binding energy occurring in the centroid of the valence band is assigned to these electrons, which are referred to as O($L_{2,3}$). The calculation of interatomic transitions Al($L_{2,3}$)O($L_{2,3}$)O($L_{2,3}$) or BB (i.e., assuming completely localized holes on one nearest-neighbor oxygen site) involves obtaining the separate terms in Eq. (4.16). To get E_B^V the XPS results of Sec. IV are used with the appropriate reference corrections to the vacuum level of the bulk crystal. From Eq. (4.14) and the optical data for atomic oxygen the total intra-atomic hole-hole interaction energy U_i can be empirically obtained. This is possible only if the ground-state configuration of oxygen in Al_2O_3 is known; since it is not, we assume that it is in the purely ionic limit, O $2s^22p^6$. The ^1D state of atomic oxygen $2s^22p^4$

(the ^3P state is forbidden in intermediate coupling theory for low-Z elements[1]) lies 5.2 eV *below* the ground state of O^{2-} [$O^{2-} \rightarrow O^{1-}$, −8.6 eV (Ref. 41); $O^- \rightarrow O$, +1.47 eV(Ref. 42); $^3P \rightarrow {}^1D$, 1.96 eV (Ref. 36)]. Therefore $U_i(O(L_{2,3})O(L_{2,3}), {}^1D) = E_B^V(O(L_2L_3), {}^1D) - 2E_B^V(L_{2,3}) = -5.2 - 2(-8.6) = 12.0$ eV. The extra-atomic cross-polarization energy $P_{xc}(O(L_{2,3})O(L_{2,3}))$ can be approximated using Eq. (4.7) and an estimation for the single-hole extra-atomic polarization energy $P_x(O(L_{2,3}))$ in Al_2O_3. Based on the relatively nonpolarizable Al nearest neighbors and loose crystal packing we estimate $P_x(O(L_{2,3})) \cong 1.5$ eV and $P_{xc}(O(L_{2,3})O(L_{2,3})) \cong 3$ eV. The energies of the Auger transitions calculated from these latter values are given in Table III.

The energy of the interatomic transition $Al(L_{2,3})O(L_{2,3})O(L_{2,3})'$ or BB' case involving delocalized holes is calculated from Eq. (4.17). Here we need only determine the total nonlocalized hole-hole interaction energy U_x given by Eq. (4.11). The average distance between the holes is taken to be the oxygen-oxygen separation in Al_2O_3. The calculated values and resulting BB' transition energies are given in Table III.

It is energetically feasible in Al_2O_3 for $O(L_1)$ electrons as well as $O(L_{2,3})$ electrons to be involved in Auger transitions. Processes BB and BB', analogous to those involving $O(L_{2,3})$ electrons, are possible and their calculation follows from Eqs. (4.16) and (4.17), respectively. The only modification occurs in calculating U_x since the final double hole-state in this BB process (assuming again the oxygen ground state is O $2s^22p^6$) is O $2s2p^5$, $^3P^0$.[36] The appropriate energies are listed in Table III.

The final interatomic Auger process that must be considered is the AB process which is the predominant mechanism for decay of $Al(L_1)$ holes in Al_2O_3. It is written in our notation as $Al(L_1)Al(L_{2,3})O(L_{2,3}$ or $L_1)$ and is referred to more specifically as an interatomic Coster-Kronig transition. Intra-atomic Coster-Kronig decay, i.e., $Al(L_1)Al(L_{2,3})Al(L_{2,3})$, *would* be more probable than the interatomic AB mechanism, but from Eq. (4.11) and the appropriate energies it is energetically forbidden. The energies of the two AB processes involving either $O(L_{2,3})$ or $O(L_1)$ electron-ejection are listed in Table III.

Calculations of interatomic transitions in MgF_2 and NaF are also given in Table III. The extra-atomic cross-polarization energy in MgF_2 was estimated to be 3 eV based on similar considerations in Al_2O_3 (the Mg^{+2} ions are more polarizable than Al^{+3} ions but the F^- ions are less so than O^{2-}). The estimated P_{xc} values for MgF_2 and Al_2O_3 are similar to that calculated[8] for NaF from the Mott-Littleton theory[33] and Eq. (4.7). The U_i energies for F^- were taken from spectroscopic data[36] using the accepted fluorine electron affinity of 3.4 eV.[43]

Transitions which are either energetically forbidden, unobservable due to obstruction from intense, low-energy secondary electrons (e.g., $Al(L_1)Al(L_{2,3})O(L_1)$ transitions), or unobservable due to interference with small impurity signals (e.g., carbon 1s electrons on MgF_2 interfere with the $Mg(K)Mg(L_1)F(2p)$ and $Mg(K)Mg(L_1)F(2s)$ transitions) have not been included in Table III.

V. DISCUSSION

The major goal of this work is to understand the phenomenology of valence-electron interatomic Auger transitions on a level comparable to that achieved for core-level intra-atomic transitions. The means by which this goal is tested involves the comparison between observed and predicted Auger energies using empirically determined one-electron binding energies. In order to evaluate the success of this comparison it is worthwhile to briefly restate the assumptions and limitations of our approach.

Ionic compounds were chosen for this study because the various energies entering into the calculation of interatomic transitions can either be empirically determined or reasonably approximated in a straightforward way. In the limit of complete ionicity, i.e., infinitely narrow valence bands, the interatomic hole-hole interaction and extra-atomic cross-polarization energies can be calculated using simple dielectric theory,[33] while the corresponding intra-atomic energies are readily obtained from optical absorption data.[36] It must be mentioned, however, that the ionic limit, and therefore the energies so determined under its assumptions, are an approximation invoked solely for computational expedience. From an experimental point of view, we recall that it was necessary to reference the Auger electron energies, measured by electron bombardment, to the same level appropriate to x-ray photoemission electron binding energies, measured by photon radiation.[44] In carrying out this procedure, an uncertainty in the absolute Auger energies of ±1.5 eV due to nonstationary charging conditions was unavoidable. Furthermore, some of the Auger energies could not be precisely determined even in a relative manner because of interference with either ubiquitous metal transitions or a rapidly varying secondary electron background.

With the above limitations and approximations in mind, we compare the observed and calculated interatomic-transition energies for Al_2O_3, MgF_2, and NaF in Table IV. For Al_2O_3 the en-

TABLE III. Summary of calculated interatomic Auger transition energies (in eV).

Compound	Transition	Notation	$E_B^V(X)$ [a]	$E_B^V(Y)$ [a]	$E_B^V(Z)$ [a]	$P_{xc}^X(YZ)$ [b]	$U_i(YZ)$ [c]	$U_x(YZ)$ [d]	$U_x(YZ)$ [e]	$E_k^V(XYZ)$
	$Al(L_{2,3})O(L_{2,3})O(L_{2,3})$	*BB*	81.9	16.0	16.0	3.0	12.0			40.9
	$Al(L_{2,3})O(L_{2,3})O(L_{2,3})'$	*BB'*	81.9	16.0	16.0			1.6		48.3
Al_2O_3	$Al(L_{2,3})O(L_{2,3})O(L_1)$	*BB*	81.9	16.0	31.0	3.0	15.4			22.5
	$Al(L_{2,3})O(L_{2,3})O(L_1)'$	*BB'*	81.9	16.0	31.0			1.6		33.3
	$Al(L_1)Al(L_{2,3})O(L_{2,3})$	*AB*	126.7	81.9	16.0				3.0	25.6
	$Mg(L_{2,3})F(L_{2,3})F(L_{2,3})$	*BB*	55.8	14.4	14.4	3.0	16.6			13.4
	$Mg(L_{2,3})F(L_{2,3})F(L_{2,3})'$	*BB'*	55.8	14.4	14.4			2.7		24.3
MgF_2	$Mg(L_1)Mg(L_{2,3})F(L_{2,3})$	*AB*	95.5	55.8	14.4				3.8	20.5
	$Mg(K)Mg(L_{2,3})F(L_{2,3})$	*AB*	1309.4	55.8	14.4				3.8	1235.4
	$Mg(K)Mg(L_{2,3})F(L_1)$	*AB*	1309.4	55.8	25.2				3.8	1214.6
	$Na(L_{2,3})F(L_{2,3})F(L_{2,3})'$	*BB'*	35.7	13.4	13.4			2.5		6.4
NaF	$Na(L_1)Na(L_{2,3})F(L_{2,3})$	*AB*	68.4	35.7	13.4				3.6	15.7
	$Na(K)Na(L_{2,3})F(L_{2,3})$	*AB*	1076.6	35.7	13.4				3.6	1024.0

[a] Empirical one-electron binding energy relative to the vacuum level, from Table I.
[b] Extra-atomic cross-polarization energy, approximated from Eq. (4.7).
[c] Empirical total intra-atomic hole-hole energy using Eq. (4.4) and values from Refs. 36 and 41–43. The L_2L_3 configuration is ^1D, the L_1L_3 configuration is $^3P^0$ (the latter value determined from extrapolation of $^3P^0$ energies in Ref. 36 of isoelectronic ions).
[d] Total nonlocalized hole-hole energy, approximated from Eq. (4.11), where R_{YZ} is the interionic distance between nearest-neighbor ligands.
[e] Same as in d, but R_{YZ} is the metal-ligand distance.

TABLE IV. Comparison between calculated and experimental interatomic Auger energies (in eV).

Compound	Transition	Notation	E_k^V(calc) [a]	E_k^V(expt) [b]	Label [b]	Δ [c]
Al_2O_3	$Al(L_{2,3})O(L_{2,3})O(L_{2,3})'$	BB'	48.3	49.0	P_1	−0.7
	$Al(L_{2,3})O(L_{2,3})O(L_{2,3})$	BB	40.9	42.0	P_2	−1.1
	$Al(L_{2,3})O(L_{2,3})O(L_1)'$	BB'	33.3	34.5	P_3	−1.2
	$Al(L_1)Al(L_{2,3})O(L_{2,3})$	AB	25.6	27.4	P_4	−1.8
	$Al(L_{2,3})O(L_{2,3})O(L_1)$	BB	22.5	(24.1)	P_5'	(−1.6)
MgF_2	$Mg(L_{2,3})F(L_{2,3})F(L_{2,3})'$	BB'	24.3	28.2	P_1	−3.9
	$Mg(L_1)Mg(L_{2,3})F(L_{2,3})$	AB	20.5	22.5	P_2	−2.0
	$Mg(L_{2,3})F(L_{2,3})F(L_{2,3})$	BB	13.4	14.4	P_3	−1.0
	$Mg(K)Mg(L_{2,3})F(L_{2,3})$	AB	1235.4	1234.1	P_5	1.3
	$Mg(K)Mg(L_{2,3})F(L_1)$	AB	1214.6	1212.9	P_6	1.7
NaF	$Na(L_1)Na(L_{2,3})F(L_{2,3})$	AB	15.7	16.0	P_1	−0.3
	$Na(L_{2,3})F(L_{2,3})F(L_{2,3})'$	BB'	6.4	7.0	P_3	−0.6
	$Na(K)Na(L_{2,3})F(L_{2,3})$	AB	1024.0	1023.4	P_4	0.6

[a] From Table III.
[b] From Table II.
[c] E_k^V(calc) − E_k^V(expt).

ergies of the five predicted transitions are in good agreement with the observed peaks labeled P_1 through P_4. The average and nearly systematic discrepancy of -1.2 ± 0.6 eV between theory and experiment lies within the uncertainty of the measurements. Inclusion of the tentatively assigned peak P_5' in the comparison modifies the average discrepancy to -1.3 ± 0.4 eV. It is tempting to point out that the assignments appear consistent with the observed broader peak P_4 relative to peaks P_1, P_2, and P_3 since additional broadening is expected for (interatomic) Coster-Kronig transitions. However, Auger peak intensities and linewidths cannot be reliably discussed at this time because of the difficulty in assessing meaningful values from a second-derivative spectrum of overlapping peaks.[46] Also in the absence of reliably calculated interatomic-transition probabilities, it is not clear as to what factors the relative transition intensities will be most sensitive.

The predicted and observed transitions for MgF_2 are in somewhat poorer agreement than found for Al_2O_3. The average discrepancy of -0.8 ± 2.3 eV is small, but the standard deviation of the mean is outside experimental uncertainties. The largest deviation is found for peak P_1 which strongly interferes with the $L_1L_{2,3}V$ transition of Mg metal (the second derivative of closely spaced peaks can give rise to misleading peak positions). Assuming the largest allowable error of ~1.5 eV in the P_1 peak assignment, an average discrepancy for all the peaks of -0.5 ± 1.9 eV is obtained. Comparison of the low-energy transitions, peaks P_1–P_3, with the high-energy transitions, peaks P_5 and P_6, show approximately the same disagreement but of opposite sign. Since the latter transitions were measured in the XPS system and therefore do not contain reference-level correction errors, this comparison suggests the limits of reliability for the values used in the energy calculations as well as in the determination of the experimental energies.

A comparison between the theoretical and experimental interatomic Auger energies for NaF shows an average discrepancy of only -0.1 ± 0.5 eV. The comparison between low- and high-energy transitions, as done for MgF_2, indicates that this good agreement is not fortuitous.

In the three crystals studied there are peaks whose energies are incompatible with the theoretically predicted transitions. There are two additional sources for such peaks. One is a final-state effect arising from overlapping energy-dependent contributions of both the secondary electron-production mechanisms and a high density of states above the vacuum level.[18] Although optical absorption data of unfilled conduction states exist for some of the systems studied[13, 14] the relative importance of these states is not straightforward to predict. The second possible source of additional peaks is from interfacial Auger transitions. These have been postulated[45, 47] to occur at the interfaces between metals and ionic crystals and might therefore be evident in our experiments. It is difficult, however, to assess their importance (and possibly their occurrence) in these or other systems because of at least two questions. First, if one accepts the assumption[45, 47] that the final-state double vacancies are sufficiently

delocalized such that hole-hole and extra-atomic cross-polarization energies are negligible, it is not clear why certain transitions are observed while others apparently are not.[45, 47, 48] Second, it has been tacitly assumed[45, 47, 48] that the stoichiometry of the crystal at the interface is the same as in the bulk, but this may not at all be the case. In view of the uncertainties regarding both the interfacial transitions and the contribution of structure to the secondary electron spectrum from unoccupied conduction states, we are unable to assign the peaks labeled with primes in Figs. 5–7.

The overall good agreement between the predicted and observed interatomic Auger energies in Al_2O_3, MgF_2, and NaF is particularly encouraging when one considers the experimental and theoretical limitations mentioned above. The fact that there exist some unidentified structures in the low-kinetic-energy spectrum of these compounds does not discredit the agreement so much as it points out the need for further study.

In summary, we have observed interatomic Auger transitions in the ionic crystals Al_2O_3, MgF_2, and NaF and have shown that the transition energies can be predicted with a simple point-charge model. In order to obtain reliable agreement between this theory and experiment it is essential to include the hole-hole interaction and polarization contributions. The good agreement obtained for both low-energy ($E < 100$ eV) and high-energy (KLV) interatomic transitions gives additional support to the basic model of empirical one-electron binding energies and point-charge corrections. Further improvements using more realistic theoretical models including band-structure effects and possible local density of states variations should provide worthwhile areas of investigation. Future, more detailed studies may be particularly important in narrow-band metals and/or surface complexes where the hole-hole interaction and polarization effects are likely to be intermediate between the simple point-ion model and a uniform electron-density bulk solid.

---

[1]For general reviews of Auger spectroscopy see K. D. Sevier, *Low Energy Electron Spectroscopy* (Wiley, New York, 1972), Chap. 3; C. C. Chang, Surf. Sci. 25, 53 (1971).

[2]G. Schön, J. Electron Spectrosc. Rel. Phenom. 2, 75 (1973)

[3]For a brief review of interatomic Auger transitions see P. H. Citrin, J. Electron Spectrosc. Rel. Phenom. 5, 273 (1974).

[4]W. Bambynek, B. Crasemann, R. W. Fink, H.-U. Freund, H. Mark, C. D. Swift, R. E. Price, and P. V. Rao, Rev. Mod. Phys. 44, 716 (1972).

[5]J. E. Rowe, H. Ibach, and H. Froitzheim, Surf. Sci. 48, 44 (1975).

[6]E. G. McRae and C. W. Caldwell, Surf. Sci. 2, 509 (1964).

[7]P. S. P. Wei, Surf. Sci. 24, 219 (1971).

[8]P. H. Citrin and T. D. Thomas, J. Chem. Phys. 57, 4446 (1972).

[9]S. M. Sze, *Physics of Semiconductor Devices* (Wiley-Interscience, New York, 1969), Chap. 8.

[10]J. Bardeen, Phys. Rev. 71, 717 (1947).

[11]S. Kurtin, T. C. McGill, and C. A. Mead, Phys. Rev. Lett. 22, 1433 (1969), and references cited therein.

[12]From Eq. (2.2) it follows that addition of a constant photoelectric threshold (however accurate or inaccurate it may be) to both the Auger and x-ray photoemission energies referenced to the valence band edge will not affect *comparisons between* the two different measurements.

[13]H. J. Hagemann, W. Gudat, and C. Kunz, J. Opt. Soc. Am. 65, 742 (1975).

[14]G. W. Rubloff, Phys. Rev. B 5, 662 (1972).

[15]A. H. Nethercot, Phys. Rev. Lett. 33, 1088 (1974).

[16]W. Pong and J. A. Smith, in *Vacuum Ultraviolet Radiation Physics* (Pergamon-Vieweg, Braunschweig, 1974), p. 383.

[17]The photoelectric threshold for MgF_2 was approximated by that determined for CaF_2 in Ref. 14. See also Ref. 12.

[18]S. Andersson, Solid State Commun. 11, 1401 (1972); V. E. Henrich, Phys. Rev. B 7, 3512 (1973).

[19]C. J. Powell and J. B. Swan, Phys. Rev. 115, 869 (1959).

[20]A. Barrie, Chem. Phys. Lett. 19, 109 (1973).

[21]T. E. Gallon and J. A. D. Matthew, Phys. Status Solidi 41, 343 (1970).

[22]D. G. Lord and T. E. Gallon, Surf. Sci. 36, 606 (1973).

[23]In Ref. 3 the vacuum level of Mg metal was used as the common reference for the x-ray photoemission and Auger energies, accounting for the differences between the results quoted in that work and those reported here.

[24]C. D. Wagner and P. Biloen, Surf. Sci. 35, 82 (1973).

[25]J. A. D. Matthew, Surf. Sci. 40, 451 (1973).

[26]S. P. Kowalczyk, R. A. Pollak, F. R. McFeely, and D. A. Shirley, Phys. Rev. B 8, 3583 (1973).

[27]P. S. Bagus, Phys. Rev. 139, A619 (1965).

[28]L. Hedin and G. Johannson, J. Phys. B 2, 1336 (1969).

[29]This term has also been called the "static relaxation energy" (see Ref. 30) to distinguish it from what was referred to as the "dynamical relaxation" of the outer electrons in the single hole-state picture. Since these terms may be interpreted by the unwary reader to imply a distinction between adiabatic versus sudden relaxation—which is certainly not the case—we have chosen a somewhat longer but less ambiguous terminology.

[30]D. A. Shirley, Chem. Phys. Lett. 17, 312 (1972).

[31]It has been argued by C. A. Nicolaides and D. R. Beck, Chem. Phys. Lett. 27, 269 (1974), that Eq. (4.4) is inadequate for open shell, low-Z atoms because of exchange interactions.

[32]For a brief review of this topic, see P. H. Citrin and D. R. Hamann, Phys. Rev. B 10, 4948 (1974).
[33]N. F. Mott and M. J. Littleton, Trans. Faraday, Soc. 34, 485 (1938).
[34]This term has also been called the "Auger extra-atomic relaxation energy" in Ref. 26. See also comment in Ref. 29.
[35]W. N. Asaad and E. H. S. Burhop, Proc. Phys. Soc. Lond. 71, 369 (1958).
[36]C. E. Moore, Natl. Bur. Stand. (U.S.), Circ. 467, Vol. 76, 81 (1949).
[37]G. Johansson, J. Hedman, A. Berndtsson, M. Klasson, and R. Nilsson, J. Electron Spectrosc. and Rel. Phenom. 2, 295 (1973).
[38]H. Körber and W. Mehlhorn, Z. Phys. 191, 217 (1966).
[39]G. Wentzel, Z. Phys. 43, 524 (1927).
[40]A calculation of interatomic transition probabilities involving an oxygen atom on the surface of sodium metal has been performed by J. A. D. Matthew and Y. Komninos, Surf. Sci. 53, 716 (1975). However, this calculation applies to a metal with only one oxygen neighbor rather than the coordination number of atoms or ions in a crystal.
[41]An average energy of 8.6± 0.2 eV for the two-electron affinity of oxygen is determined from the one-electron affinity, Ref. 42, and averaged lattice data, M. P. Tosi, Solid State Phys. 16, 65 (1964).
[42]L. M. Branscomb, in *Atomic and Molecular Processes*, edited by D. R. Bates (Academic, New York, 1962).
[43]R. S. Berry and C. W. Reimann, J. Chem. Phys. 38, 1540 (1963).
[44]Because the need for this reference-level procedure was not recognized in earlier interatomic Auger studies (for example, see Refs. 21 and 45), the predicted energies in those works are only very approximate.
[45]A. P. Janssen, R. C. Schoonmaker, A. Chambers, and M. Prutton, Surf. Sci. 45, 45 (1974).
[46]The majority of other Auger studies have used the first derivative technique for measuring peak intensities and positions. This is an even more unreliable procedure than the second-derivative technique because peak positions determined by the former method depend on the width of the peaks and because variations in the secondary background are less easily suppressed.
[47]A. P. Janssen, R. Schoonmaker, J. A. D. Matthew, and A. Chambers, Solid State Commun. 14, 1263 (1974).
[48]H. D. Shih, K. O. Legg, and F. Jona, Surf. Sci. 54, 355 (1976).

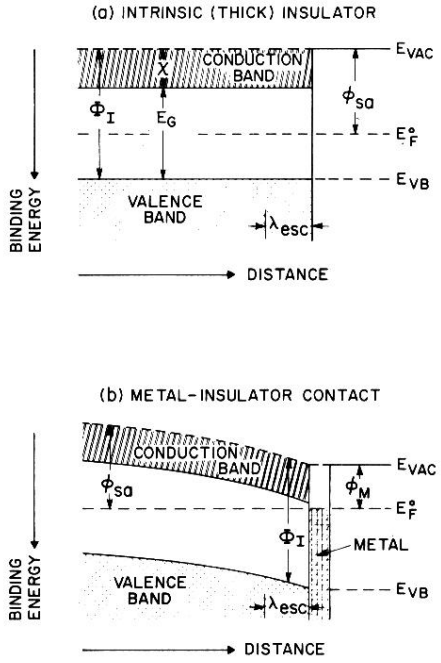

FIG. 1. Energy-level diagrams for (a) intrinsic insulators showing quasi-Fermi level near the center of the forbidden gap and for (b) a metal-insulator contact in the usual Schottky limit of no interface states. For the latter case the Fermi level is determined by the metal and not by the insulator.